CHAPTER 4

DESIGN AND PERFORMANCE ANALYSIS OF PCM INTEGRATED SAH

CHAPTER 4

DESIGN AND PERFORMANCE ANALYSIS OF PCM INTEGRATED SAH

4.1 Introduction

SAH is a form of a heat exchanger that transfers heat to air after absorbing sun light with an absorber. In SAH, heat is transferred from an energy source (sun) to the SAH system (glass cover) by radiation and absorber plate to the air stream by convection. SAHs are commonly used for low and moderate temperature applications such as drying fabrics, drying grains, fruits, vegetables, tea, space heating, seasoning of wood, curing of industrial products, and they may also be used efficiently for curing/drying of concrete/clay building components. Because of its low material and cost demands the SAH is an important component of solar heating systems. SAH's thermal efficiency is typically lower as compared to solar water heaters due to their naturally poor heat transfer capacities between the plate that absorbs heat and air moving through the duct. SAH thermal efficiency must be enhanced to make them commercially viable by increasing the heat transfer coefficient [1-4]. Improving the thermal performance of SAH remains a difficult challenge for both manufacturers and researchers. The heat transfer coefficient determines the heat transmission rate between the fluid and absorber plate. Researchers use the influence of turbulators with various shapes to enhance the thermal performance of SAH. Design factors, shapes employed, conditions of flow and their impact on turbulent conditions, the transfer of heat rate, absorber temperatures, and thermo-hydraulic enhancing factor are some of the approaches addressed for improving the performance of SAH [5]. The loss of heat increases with lengthy and complex process, like the direct proportional relationship between wire length and resistance in electricity laws. Thus, SAH and PCM non-integrated systems need additional insulating material, space, and increases the cost of the system. Because of its multiple phases and components, non-integrated systems cost more to maintain. Many researchers investigated SAH using storage material like PCM for such reasons [6]. The use of PCM by the SAH enhances the thermal performance of the SAH regardless of the absorber plate configuration [7]. To use a SAH beyond peak sunlight hours, it is recommended to combine it with a TESS. Optimising the architecture of TESS is one way to improve the thermal efficiency of SAH when it is used in combination with TESS. The total flow rate and intake temperature of the air, the kind of PCM, the positioning, and the diameters of the tubes each have an impact on the TESS design optimisation process [8].

The study of single and dual pass finned plate SAHs with a wire built of steel mesh revealed that the thermal efficiency of these devices improved as the air mass velocity increased. Additionally, it is found that the thermal efficiency of the double-pass collector is higher than that of the single-pass collector [9]. Application of PCM in window units reduces building energy consumption and enhances solar energy use. The thermal performance of double-glazing units examined in relation to PCM thickness and melting temperature originates that when PCM thickness reaches 50mm, compared to 4mm, inner surface temperature rises by 158.7%, total transmitted energy falls by 109.1%, and solar energy is lost by 86.1%. As a result, a PCM container thickness of 12-30 mm and a melting temperature of 14-16 ºC are recommended [10].

Keeping in view of the above, and the results of characterization of the three selected PCMs from the previous Chapter. The present Chapter includes the study of suitability of these three specific PCMs (acetamide, stearic acid and paraffin wax) for integration in SAH. Comprehensive understanding of suitability of these PCMs require a thorough study based on the fundamental laws of heat transfer and incorporating material properties, geometry of the proposed SAH and weather conditions profile. The study involves determination of the design parameters (mass flow rate, length of the absorber and PCM sizing) of PCM integrated SAH through a series of simulations. Subsequently PCMSAH is developed based on design parameters from simulation for optimum theoretical outlet temperature. Further, comparative performance analysis of the selected PCMs incorporated in SAH has also been studied using standard experimental procedures. The validation of experimental and theoretical outlet temperature is confirmed. The detailed energy analysis such as useful, absorbed, lost, and stored heat is evaluated for the SAH with and without PCM. The uncertainty analysis for thermal efficiency of the PCMSAH is determined to estimate the accuracy of the experiments performed on the PCMSAH.

4.2 Materials and Methods

4.2.1 Geographical location of experimental site

Tezpur University campus (Fig. 4.1) which is situated in the North Bank Plain Zone of Assam, India (26.7003 ° N and 92.8308 ° E) with 4.5-5.0 $kWhm^{-2}day^{-1}$ annual average global horizontal irradiance (GHI) is the location of the experimental site [11].

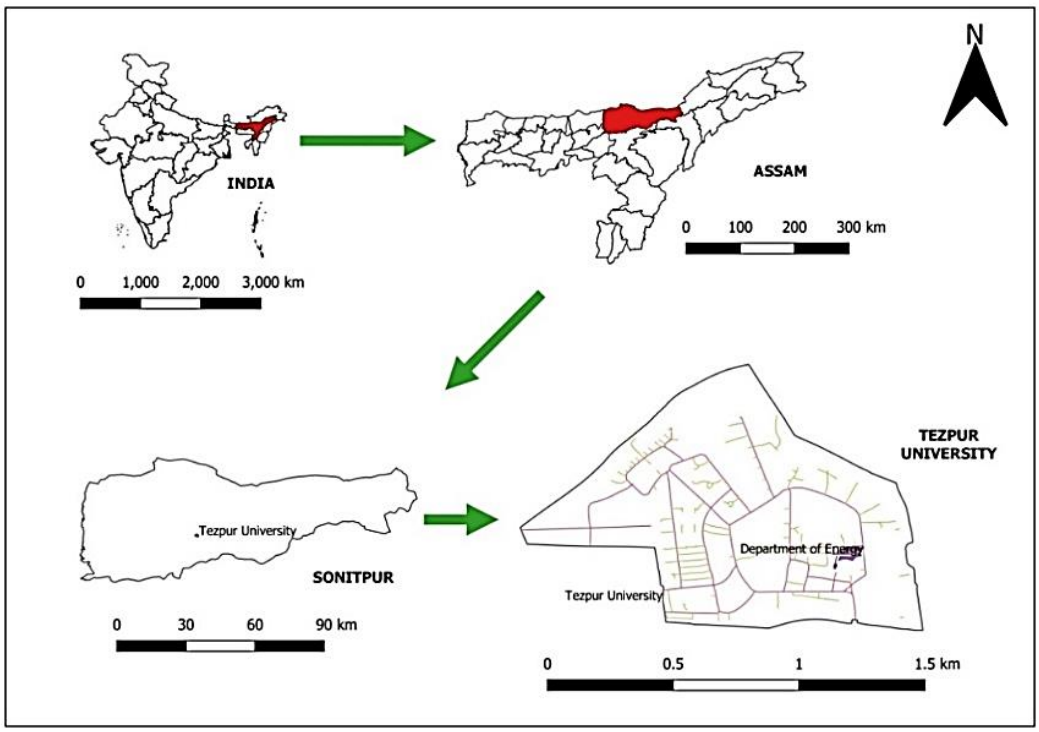

Fig. 4.1: Location of the experimental site

4.2.2 Design of PCMSAH

The conceptual layout of the proposed PCM integrated flat plate collector type SAH is presented in Fig. 4.2, which consists of (i) a glass cover of high transmissivity to solar radiation, (ii) an absorber plate with high absorptivity on its upper surface and lower face carrying PCM and (iii) insulation layer around the absorber plate. The design parameters of the proposed PCMSAH are determined/selected using standard procedures aiming to achieve the best thermal performance as discussed below.

4.2.2.1 Sizing of PCMSAH

Sizing of PCMSAH unit is described by three key parameters viz., (i) length of air flow path, (ii) mass flow rate of air, and (iii) quantity of PCM. These parameters are determined using the fundamental principle of energy conservation for the proposed PCMSAH as depicted through thermo-schematic diagram of the PCMSAH in Fig. 4.2. The relationships representing different components of thermal energy during the operation of the PCMSAH available in literature are used for the analysis. Some of the relevant assumptions are (i) Perpendicular to the air circulation, there is no sedimentation (ii) For long-wavelength radiation at an equivalent sky temperature, the sky is treated as a black body (iii) The glass

cover, absorbent plate, and insulation have insignificant heat capabilities (iv) The storage medium has an average temperature $T_{st}(t)$ at a time t, and there is no temperature gradient across the thickness of the glass cover. This assumption can be met by keeping the storage material's thickness low, and (v) There is no air leakage from the collector since the system is fully insulated.

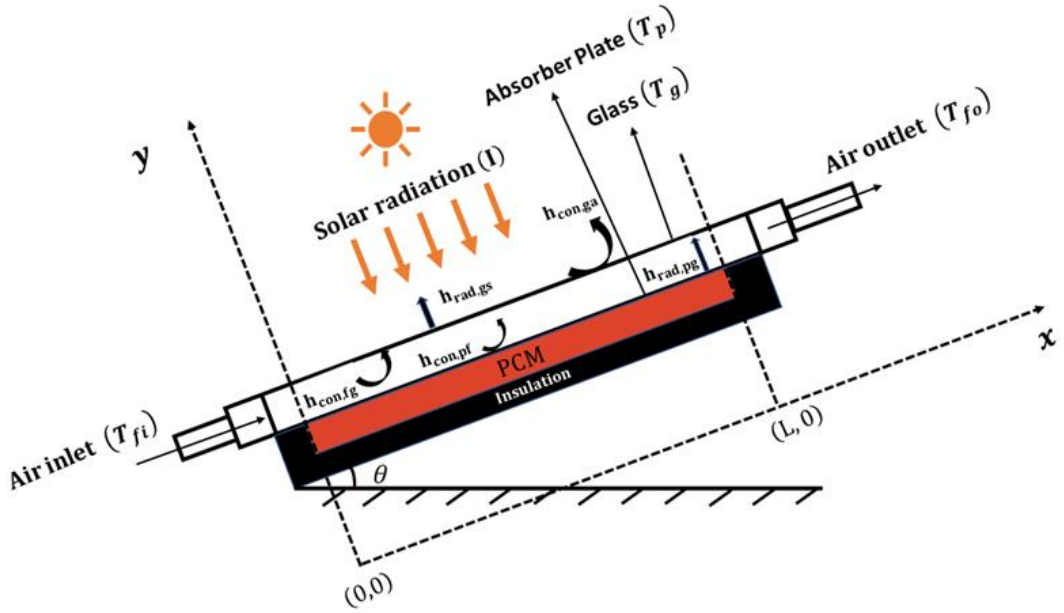

Fig. 4.2: Thermo-schematic diagram of the PCMSAH

4.2.2.2 Energy balance for design of PCMSAH

Energy balance equation for the four components of thermal energy *viz*., absorbed heat (Q_A), useful heat (Q_u), stored heat (Q_{st}) and lost heat (Q_{loss}) for the PCMSAH [12] are given as below.

$$Q_A = Q_u + Q_{st} + Q_{loss} \tag{4.1}$$

Parametric equations are used to represent Q_A, Q_u, and Q_{loss} in terms of thermo-physical properties of the system components, coefficients of heat transfer, operating conditions including input solar insolation and ambient conditions for operation of the PCMSAH.

The absorbed heat Q_A is the heat absorbed from the solar radiation (I) by an absorber plate with an area A_p received through a glass cover having transmissivity (τ_g) and absorptivity (α_g) is estimated as below.

$$Q_A = A_p(\tau_g \alpha_g)I \tag{4.2}$$

The useful heat (Q_u) is estimated from the heat gain by the air with mass flow rate ($\dot{m}$), specific heat of air (C_p) at the mean temperature between inlet (T_{ci}) and the outlet temperature (T_{co}) of the air as given below.

$$Q_u = \dot{m}\, C_p(T_{co} - T_{ci}) \tag{4.3}$$

The following continuity equation is used to express mass flow rate of air passing through PCMSAH where ρ is the density of the air, V_{av} is the velocity of the air and A_c is the area of the entrance channel.

$$\dot{m} = \rho\, V_{av} A_c \tag{4.4}$$

The thermal efficiency of the SAH with and without PCM can be estimated as below.

$$\eta = \frac{Q_u}{Q_A} \times 100\% \tag{4.5}$$

where, (Q_u) is the useful heat gained and (Q_A) is the absorbed heat by the PCMSAH.

The heat lost from SAH is given below [12].

$$Q_{loss} = U_{loss} A_p (T_p - T_a) \tag{4.6}$$

where, U_{loss} is the collector's overall heat loss coefficient which is equal to sum of the heat loss coefficients through the top U_t, the bottom U_b and the edges U_e of the collectors as given below. Thermal energy is lost from the collector to the environment via conduction, convection, and infrared radiation.

$$U_{loss} = U_t + U_b + U_e \tag{4.7}$$

The top loss coefficient between the SAH and the outside.

$$U_t = \left(\frac{1}{h_{con,pg} + h_{rad,pg}} + \frac{1}{h_w + h_{rad,ga}} \right)^{-1} \tag{4.8}$$

where, $h_{con,pg}$ is the convective heat transfer coefficient between the absorber and the glass cover, $h_{rad,pg}$ is the radiation heat transfer coefficient within the absorber plate and glass cover, h_w is the heat transfer coefficient in the glass cover top owing to external wind velocity and $h_{rad,ga}$ is the radiation heat transfer coefficient from the glass cover to the ambient respectively.

The following equation can be used to compute the convective heat transfer coefficient between the absorber and the glass cover [12].

$$h_{con,pg} = Nu\frac{\mathrm{k}}{d_f} \tag{4.9}$$

The Nusselt number can be derived from three-region correlation of Buchberg et al. [13] as expressed below.

$$Nu = 1 + 1.446(1 - \frac{1708}{Ra'})^{+} \text{ for } 1708 \leq Ra' \leq 5900 \tag{4.10}$$

(The + bracket goes to zero when negative),

$$Nu = 0.229\ (Ra')^{0.252} \text{ for } 5900 \leq Ra' \leq 9.23 \times 10^4 \tag{4.11}$$

$$Nu = 0.157(Ra')^{0.285} \text{ for } 9.23 \times 10^4 \leq Ra' \leq 10^6 \tag{4.12}$$

where, $Ra' = Ra\cos\theta$ denotes the Rayleigh number for inclined air layers. The Rayleigh number is given for natural convection flow between parallel plates (absorber plate and glass cover) as.

$$Ra = Gr \times Pr = \left[\frac{g(T_p - T_g){d_f}^3}{T_{mpg}\mu^2}\right]Pr \tag{4.13}$$

where, g is the acceleration due to gravity, T_p is the absorber plate temperature, T_g is the glass cover temperature, T_{mpg} is the mean temperature between absorber plate and glass cover, d_f is the distance between the absorber plate and glass cover, μ is the kinematic viscosity of the air and Pr is the Prandtl number given by:

$$Pr = \frac{\mu}{\alpha'} \tag{4.14}$$

where, μ and α' are the kinematic viscosity and thermal diffusivity of the air.

$$\alpha' = \frac{k}{\rho C_p} \tag{4.15}$$

For the corresponding (inlet and outlet) mean temperature (T_m), the thermo-physical characteristics of the air are taken into account. For computations, the following thermo-physical property relationships considered are specific heat (C_p), thermal conductivity (k), kinematic viscosity (μ), and density (ρ) [14].

$$C_p = 1006\left(\frac{T_m}{293}\right)^{0.0155} \tag{4.16}$$

$$k = 0.0257\left(\frac{T_m}{293}\right)^{0.86} \quad (4.17)$$

$$\mu = 1.81 \times 10^{-5}\left(\frac{T_m}{293}\right)^{0.735} \quad (4.18)$$

$$\rho = 1.204\left(\frac{T_m}{293}\right) \quad (4.19)$$

where, T_m is the mean temperature between inlet and outlet of the PCMSAH collector.

The equation below can be used to compute the radiation heat transfer coefficient within the absorber plate and glass cover [12].

$$h_{rad,pg} = \frac{\sigma\,(T_p^2+T_g^2)(T_p+T_g)}{(\frac{1}{\varepsilon_p}+\frac{1}{\varepsilon_g}-1)} \quad (4.20)$$

where, σ is the Stefan Boltzmann constant, T_p is the absorber plate temperature, T_g is the glass cover temperature, ε_p is the emissivity of the absorber plate and ε_g is the emissivity of the glass cover respectively.

The correlation used to calculate the heat transfer coefficient in the glass cover top owing to external wind velocity is provided as below [12].

$$h_w = 5.67 + 3.86V_o \quad (4.21)$$

where, V_o is the wind velocity.

The radiation heat transfer coefficient from the glass cover to the ambient is given by [12].

$$h_{rad,ga} = \varepsilon_g\sigma(T_g^2 + T_{sky}^2)(T_g + T_{sky}) \quad (4.22)$$

where, $T_{sky} = 0.0552T_a^{1.5}$ (4.23)

T_a is the ambient temperature.

The energy loss equation through the bottom U_b and the edges U_e are as follows [12].

$$U_b = \frac{k_b}{\delta_b} \quad (4.24)$$

where, k_b is the thermal conductivity of the bottom insulation material and δ_b is the thickness of the bottom insulation material.

$$U_e = \frac{(L_1+L_2)L_3k_e}{(L_1L_2\delta_e)} \quad (4.25)$$

where, L_1 is the length of the collector, L_2 is the width of the collector, L_3 is the depth of the collector, k_e is the thermal conductivity of the edge insulation material, and δ_e is thickness of the edge insulation material.

The energy balance equation for glass cover is given by [15].

$$I\alpha_g A_g + A_g h_{rad,pg}(T_p - T_g) + A_g h_{con,fg}(T_f - T_g) = A_g h_{con,ga}(T_g - T_a) + A_g h_{rad,gs}(T_g - T_{sky}) \quad (4.26)$$

where, I is the solar radiation, α_g is the absorptivity of the glass cover, A_g is the area of the glass cover, $h_{rad,pg}$ is the radiation heat transfer coefficient between the plate and the glass cover, T_p is the temperature of the absorber plate, T_g is the temperature of the glass cover, $h_{con,fg}$ is the convective heat transfer coefficient between the fluid (air) and the glass cover, T_f is the temperature of the fluid (air), $h_{con,ga}$ is the convective heat transfer coefficient between the glass cover and the ambient, T_a is the ambient temperature, $h_{rad,gs}$ is the radiation heat transfer coefficient between the glass cover and the sky and

T_{sky} is the sky temperature respectively.

The energy balance equation for air stream flow along an elemental length *dx* and *b* as the width of the absorber plate may be written as.

$$h_{con,pf}(T_p - T_f)bdx = \dot{m}c_p \frac{\partial T_f}{\partial x}dx + d_f \rho_f c_p \frac{\partial T_f}{\partial t}bdx + h_{con,fg}(T_f - T_g)bdx + U_e(T_f - T_a)bdx \quad (4.27)$$

The following are the energy balance equations of the absorber plate and storage material (PCM) [15].

The energy balance for absorber plate is given by.

$$I\tau_g \alpha_p A_p = A_p h_{rad,pg}(T_p - T_g) + A_p h_{con,pf}(T_p - T_f) + Q_{st} \quad (4.28)$$

where, τ_g is the transmissivity of the glass cover, A_p is the area of the absorber plate, $h_{rad,pg}$ is the radiation heat transfer coefficient between absorber plate and the glass cover and Q_{st} is the heat produced by the PCM storage.

Now in case of charging the temperature of PCM rise and starts melting. Therefore, Q_{st} heat produced in case of charging becomes $Q_{st,ch}$ which can be equated as:

$$Q_{st,ch} = \left(\frac{k_p}{z_p}\right) A_p\left(T_p - T_{st}\right) = \left(A_p + A_b\right)(T_{st} - T_a) + Q_{ch} \quad (4.29)$$

where, (k_p) is the thermal conductivity of the absorber plate, (z_p) is the thickness of the absorber plate, (A_p) is the area of the absorber plate, (A_b) is the area of the bottom insulation, (T_p) is the temperature of the absorber plate, (T_{st}) is the temperature of the PCM, (T_a) is the temperature of the ambient air and (Q_{ch}) is the further simplification form of heat production during charging of PCM which is given as.

$$Q_{ch} = M\left[\int_{ini\_ch,PCM}^{F_{ic}} C_{st,s}(T)\, dT + L_F + \int_{F_{fc}}^{fin\_ch,PCM} C_{st,l}(T)\, dT\right] \quad (4.30)$$

where, M is the mass of the PCM, ini_ch, PCM is the temperature of the PCM during initial charging process, F_{ic} is the temperature of the PCM at the end of the initial charging process, $C_{st,s}$ is the specific heat of the PCM in solid state, L_F is the latent heat of fusion of PCM, fin_ch, PCM is the temperature of the PCM during the final charging process, F_{fc} is the temperature of the PCM at the end of the final charging process, T is the function for temperature of the PCM and $C_{st,l}$ is the specific heat of the PCM in liquid state respectively.

Similarly, Q_{st} heat produced during discharging when the PCM stars to solidify becomes $Q_{st,dis}$ which can be equated as can be written as:

$$Q_{st,dis} = \left(\frac{k_p}{z_p}\right) A_p\left(T_p - T_{st}\right) = \left(A_p + A_b\right)(T_{st} - T_a) + Q_{dis} \quad (4.31)$$

where, Q_{dis} is the further simplification form of heat production during discharging of PCM.

$$Q_{dis} = M\left[\int_{ini\_dis,PCM}^{F_{id}} C_{st,l}(T)\, dT + L_F + \int_{F_{fd}}^{fin\_dis,PCM} C_{st,s}(T)\, dT\right] \quad (4.32)$$

where, M is the mass of the PCM, ini_dis, PCM is the temperature of the PCM during initial discharging process, F_{id} is the temperature of the PCM at the end of the initial discharging process, $C_{st,l}$ is the specific heat of the PCM in liquid state, L_F is the latent heat of fusion of PCM, fin_dis, PCM is the temperature of the PCM during the final discharging process, F_{fd} is the temperature of the PCM at the end of the final discharging process, T is the function for temperature of the PCM and $C_{st,s}$ is the specific heat of the PCM in solid state respectively.

So, now Eqs. (4.26) & (4.28) are solved to compute temperature of absorber plate (T_p) and temperature of glass cove (T_g) and put its values into Eq. (4.27) that finally results in Eq. (4.33) as given below [15].

$$\frac{\partial T_f}{\partial x} + a_1 \frac{\partial T_f}{\partial t} + b_1 T_f = f_1(t) \tag{4.33}$$

where,

$$a_1 = d_f \rho_f \, b/\dot{m} \tag{4.34}$$

$$b_1 = (b/\dot{m}C_f)\left(h_{con,pf}c2 - h_{con,pf} - h_{con,fg} + h_{con,fg}e5 - U_e + h_{con,fg}e4c2\right) \tag{4.44}$$

where, C_f is the specific heat of fluid (air) moving within the PCMSAH and convective heat transfer coefficients due to plate to fluid ($h_{con,\,pf}$) and fluid to glass ($h_{con,\,fg}$).

And

$$f_1(t) = \left(\frac{b}{\dot{m}c_p}\right)\left(d1 + d2T_a + d3T_{sky} + d4T_{st}\right) \tag{4.45}$$

Where $f_1(t)$ is the average value over a short time and may be treated as a constant because response on the PCMSAH for the metrological data of the given location is invariant for short period of time. The coefficients used in the expression of $f_1(t)$ can be referred from Appendix 4A.

The initial and boundary conditions of PCMSAH are $T_f(x = 0, t = 0) = T_{fi}$ and $T_f(x = 0) = T_{fi}$ *to* $T_f(x = L) = T_{fo}$ as shown in Fig. 1. The solution of Eq. (4.33) can be derived by transformation relation, which is given in reference [15].

The following analytical equation is generated for the average temperatures at flowing air along the length of SAH.

$$T_{fos} = \left(\frac{1}{L}\right)\int_0^L T_f(x,t)dx = \frac{f_1(t)}{b_1} + \frac{2f_1(t)}{Lb_1^2} exp\left[-\left(\frac{b_1 t}{2a_1}\right)\right]\left[exp\left(-\frac{b_1 L}{2}\right) - 1\right] + \frac{2Tf_1}{b_1 L} exp\left[-\left(\frac{b_1 t}{2a_1}\right)\right]\left[1 - exp\left(-\frac{b_1 L}{2}\right)\right] \tag{4.46}$$

A transient analytical model is used to investigate the PCMSAH, in which the temperature of fluid (air) is expected to alter with time and length of the absorber plate. The

temperatures of SAH elements and the thermal storage material (PCM), are calculated using analytical expressions. To evaluate the theoretical performance of the PCMSAH, a MATLAB simulation is utilised to solve the energy balance equations.

The input parameters to the program are the (i) design parameters, (ii) operational parameters, (iii) thermophysical properties of the PCM and (iv) climatic condition such as solar radiation, ambient temperature, and wind speed of a representative day (24/04/2019) in Tezpur (India) given in Fig. 4.3. Effects of design parameters of the SAH such as length of absorber (L) varying from 1m to 3m with an increment of 0.5 m, mass flow rate ($\dot{m}$) varying from 0.018 to 0.048 kg/s with an increment of 0.010 kg/s, types of the PCM (acetamide, stearic acid and paraffin wax) and quantity on the temperatures of the air along the length of SAH are studied. Table 4.1 summarizes the values for different parameters used for numerical calculations.

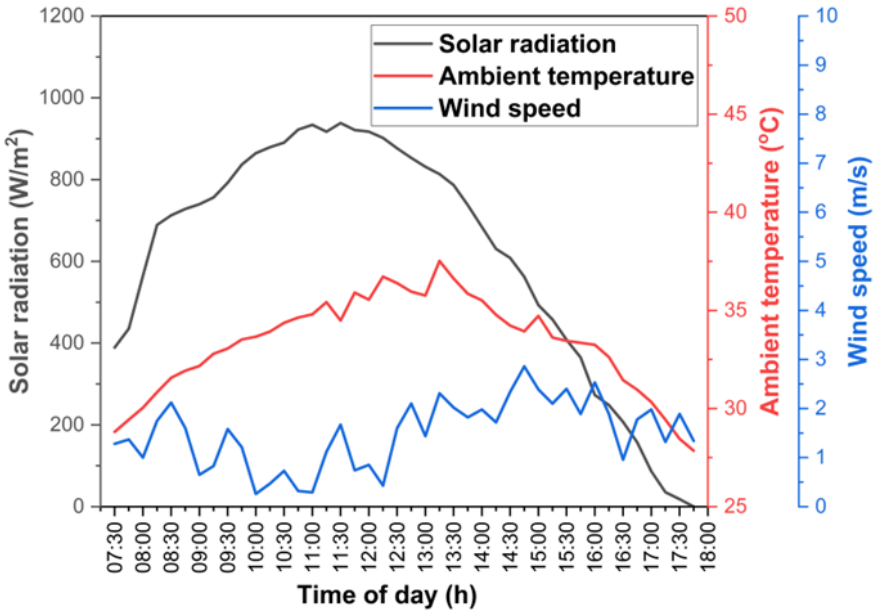

Fig. 4.3: Solar radiation, ambient temperature, and wind speed in the experimental site

Table 4.1: Parameters used in numerical computations

Parameter	value	Parameter	Value
Transmissivity of the glass cover, τ_g	0.90 [16]	Thermal conductivity of the absorber plate, k_p	1.36 W/mK [19]
Absorptivity of the glass cover, α_g	0.05 [16]	Stefan Boltzmann constant, σ	5.669×10^{-8} W/m^{2}K^4
Absorptivity of the absorber plate, α_p	0.96 [17]	Bottom insulation thickness, δ_b	0.07 m
Wind velocity, V_o	1 m/s	Edge insulation thickness, δ_e	0.07 m
Distance between the absorber plate and the glass cover, d_f	0.1 m	Width of the entrance channel or air vent, b	1 m
Angle of inclination of the collector, θ	26.70º	Emissivity of the glass cover, ε_g	0.92 [20]
Thickness of the absorber plate, Z_p	0.01 m	Emissivity of the absorber plate, ε_p	0.95 [20]
Thermal conductivity of the insulation material of bottom and edge, k_b=k_e	0.022 W/mK [18]		

The sizing of the PCM cavity determines the depth of the PCM melted from which we can quantify the amount of PCM required for the PCMSAH. Table 4.2 displays the thermophysical characteristics of three distinct PCMs that are employed in PCM cavity sizing and the differential scanning calorimetry for the thermophysical properties of the PCMs are shown in Fig. 4.4. To estimate the necessary PCM melting depth it is assumed that the PCM can be described as a lumped parameter system. Recognizing the PCM volume as Ad_{PCM}, where d_{PCM} is the depth of PCM melted, and that the first order equation gives rise to a time constant, τ_c for melting, an estimate for the depth can be derived as below [21]:

$$d_{PCM} = \tau_c/\rho_{PCM}L_{st}[I - \dot{m}c_p/A(T_{out} - T_{in}) - (U_t + U_b)(T_p - T_a)] \quad (4.47)$$

The quantity $(T_{f,o(\tau c)} - T_{f,o,initial})/(T_{f,o,\infty} - T_{f,o,initial})$ takes certain amount of time known as time constant, (τ_c) to change from 0 to 0.632. Where $T_{f,o(\tau c)}$ represents the PCMSAH outlet temperature at a certain moment, $T_{f,o,\infty}$ represents the outlet temperature at the end of the specified period, and $T_{f,o,initial}$ represents the PCMSAH outlet temperature at the beginning of the chosen period [22].

Table 4.2: Thermo-physical properties of different PCMs [23-26]

PCM	Melting Temperature (ºC)		Latent heat (kJ/kg)		Specific heat (kJ/kgK)	Thermal conductivity (W/mK)	Density (kg/m^3)
	Experiment	Literature	Experiment	Literature			
Paraffin wax	65.8	58-60	198.7	226	2.95 (solid) 2.51 (liquid)	0.24	818 (solid) 760 (liquid)
Acetamide	112.8	80.3-82	210.21	242	1.98	0.592	1159 (solid) 998.6 (liquid)
Stearic acid	63.4	54-56	200.7	186.50	2.83 (solid) 2.38 (liquid)	0.18	1080 (solid) 1150 (liquid)

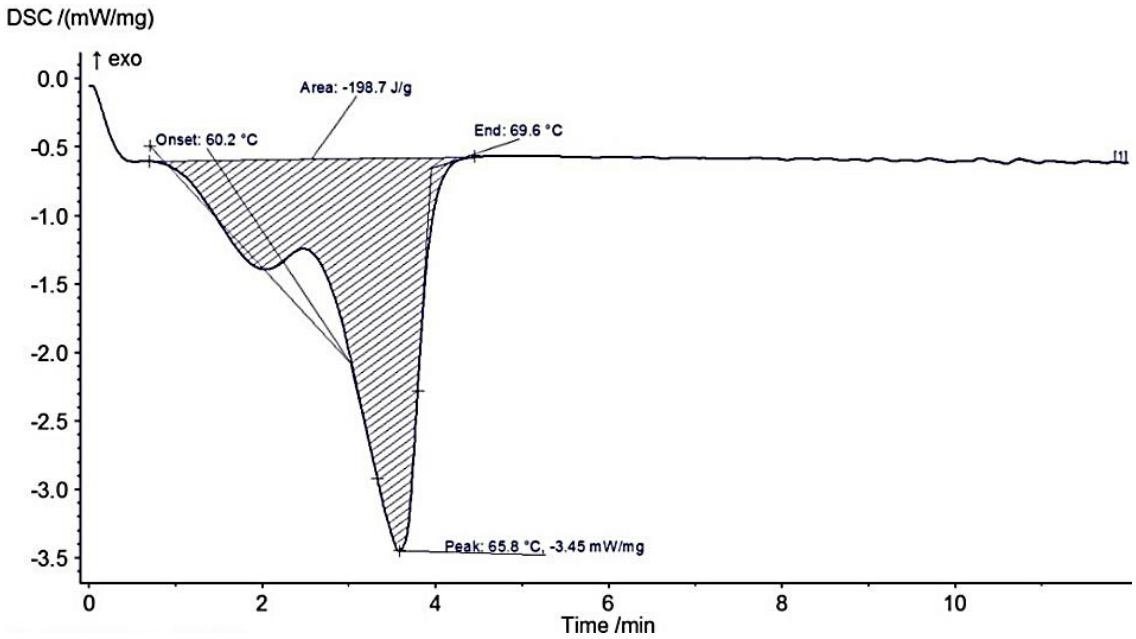

(a) Paraffin wax

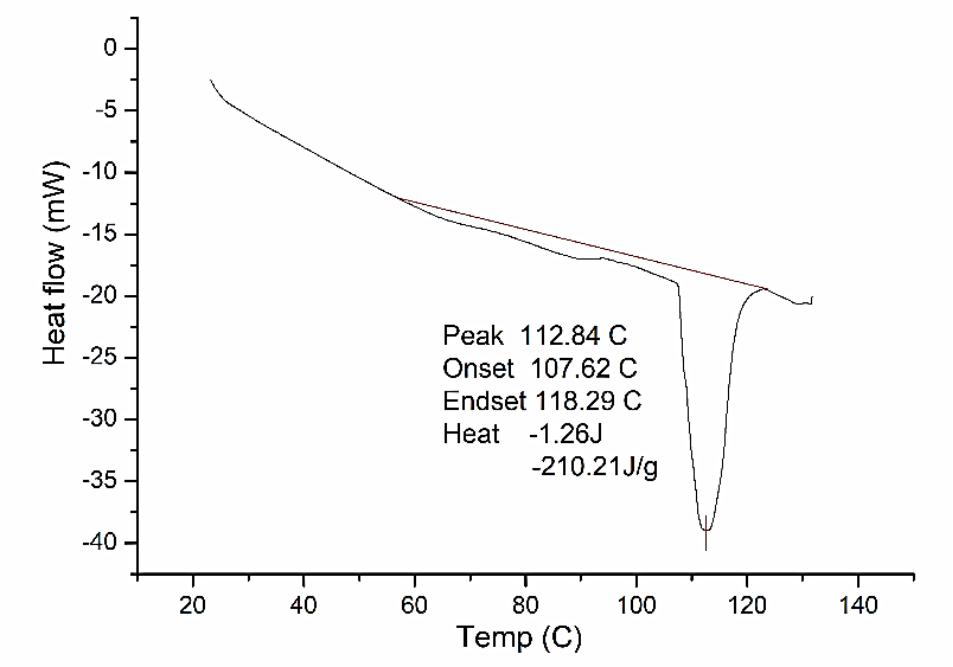

(b) Acetamide

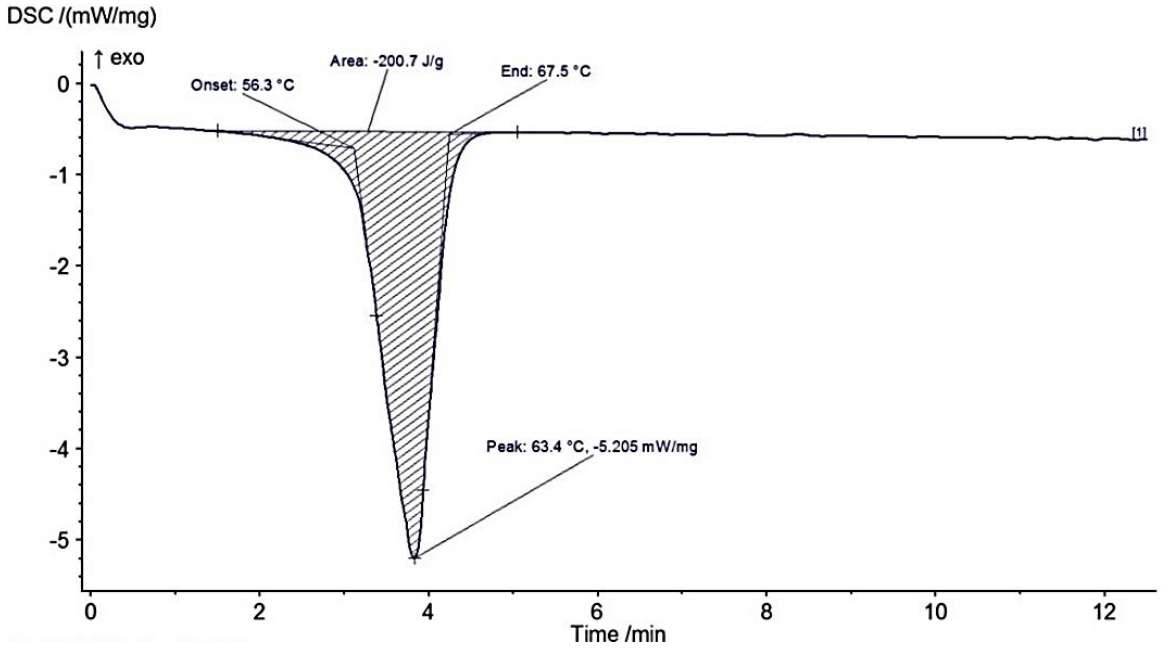

(c) Stearic acid

Fig. 4.4: DSC curve of (a) paraffin wax (b) acetamide and (c) stearic acid for melting point and latent heat of fusion value

4.2.3 Performance evaluation of designed PCMSAH

Two identical solar hot air generators (SAH) one with PCM and other without PCM is designed and developed locally in the Department of Energy, Tezpur University based on the parametric study to optimise length, mass flow rate and mass of the PCMs.

The experimental set-up is developed to investigate the performance of the SAH with or without PCM operated simultaneously throughout the day on open loop flow mode. The measurements of different parameters are performed according to the standard test procedure [27]. The temperature at different points in SAH is measured with *K* type thermocouple with ±2.2 ºC/±0.75% error as shown in Fig. 4.5. The solar radiation is measured with global solar radiation meter Kipp and Zonen with measuring capacity up to 2000 W/m^2 and relative error of ±5 w/m^2. Two similar centrifugal blowers, Forte' with 220 V/50Hz voltage/frequency, no load speed of 0 – 13000 rpm, power 600 W and blowing rate 0-2.8 m^3/min are used to give a forced draft to both the SAH. Anemometer, Testo 417 is used for measuring wind velocity with ± (0.1 m/s+1.5% of mv) relative error. Temperature data logger, Personal Daq/56TM is used for retrieving all the temperature data.

Comparative performance assessment of the two identical SAH one without PCM and another for three different PCMs viz, acetamide, stearic acid and paraffin wax are conducted on three different days of April, June, and July 2021 respectively. All the temperatures located in necessary locations as tabulated in Table 4.3, solar radiation and wind velocity are recorded throughout the day with an interval of 15 mins.

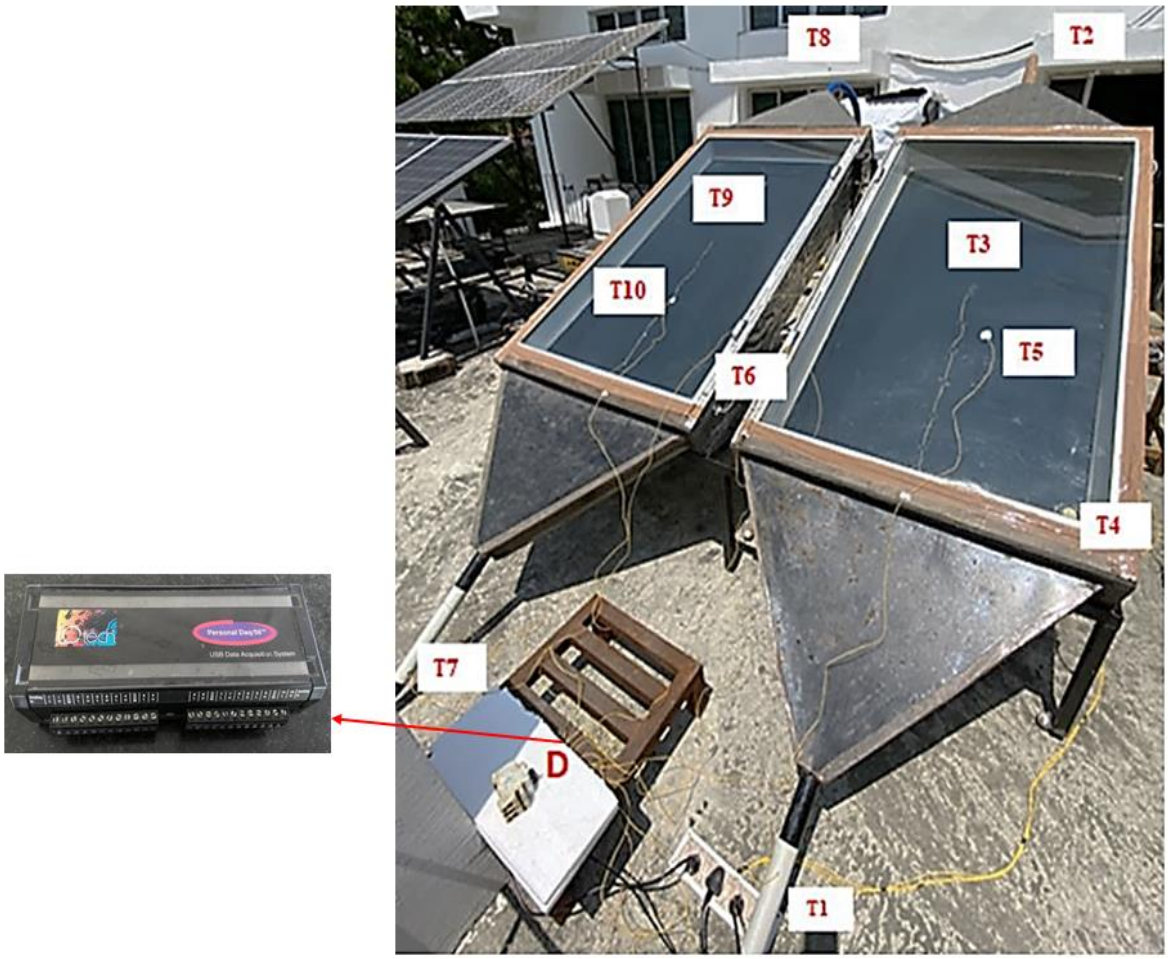

Fig. 4.5: Solar air heater with and without PCM

Table 4.3: Different Locations of thermocouples during performance test

Thermocouples	Specific measuring locations
T1	Inlet Temperature (PCM)
T2	Outlet Temperature (PCM)
T3	Plate Temperature (PCM)
T4	PCM Temperature
T5	Glass Temperature (PCM)
T6	Ambient Temperature
T7	Inlet Temperature (without PCM)
T8	Outlet Temperature (without PCM)
T9	Plate Temperature (without PCM)
T10	Glass Temperature (without PCM)
D	Temperature Data logger (Personal Daq/56TM)

4.3 Results and Discussions

The PCMSAH is designed and developed in the department of Energy, Tezpur University. The performance evaluation of SAH with and without the PCM is carried out for three clear days during the period of April to July 2021. All the experiments are conducted under the climatic condition of Tezpur, Assam, India.

4.3.1 Effect of theoretical outlet temperature of PCMSAH with varying air mass flow rate and absorber plate length

Theoretical outlet temperatures (T_{fos}) of PCMSAH with varying absorber length at different air mass flow rates are solved using Eq. (4.46) and plotted as shown on Fig. 4.6, 4.7, and 4.8 for acetamide, stearic acid and paraffin wax respectively. Outlet temperature of fluid for varying absorber length (L=1 to 3 m with the increment of 0.5 m) and with four levels of mass flow rates (viz., 0.018 kg/s, 0.028 kg/s, 0.038 kg/s and 0.048 kg/s) are plotted with time of operation in these plots.

The mass flow rate of air when increased from 0.018kg/s to 0.048kg/s resulted drop of outlet temperature by 1.81 ºC, 1.87 ºC and 1.87 ºC for acetamide, stearic acid and paraffin wax, respectively while assessing for a 3 m long absorber plate. Now, with increase in length from 1 to 3m the maximum outlet temperature difference is obtained at the lowest mass flow rate of 0.018 kg/s, and the temperature difference is found out to be 1.93 ºC in case of acetamide and 1.99 ºC in case of stearic acid and paraffin wax. Lowest outlet temperature difference is obtained with high mass flow rate of 0.048kg/s which are 0.07 ºC, 0.08 ºC and 0.09 ºC for acetamide, stearic acid and paraffin wax.

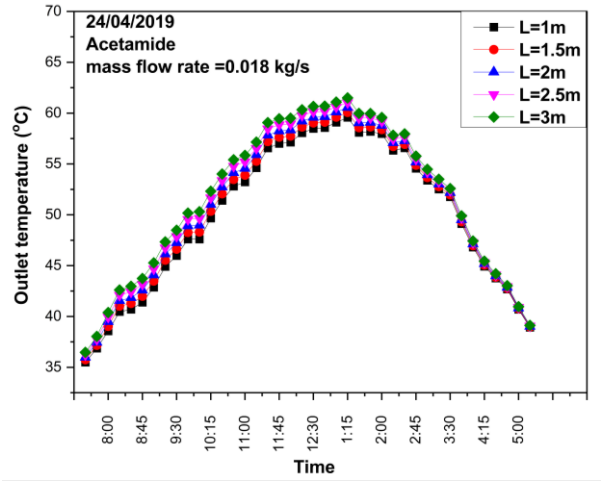

(a)

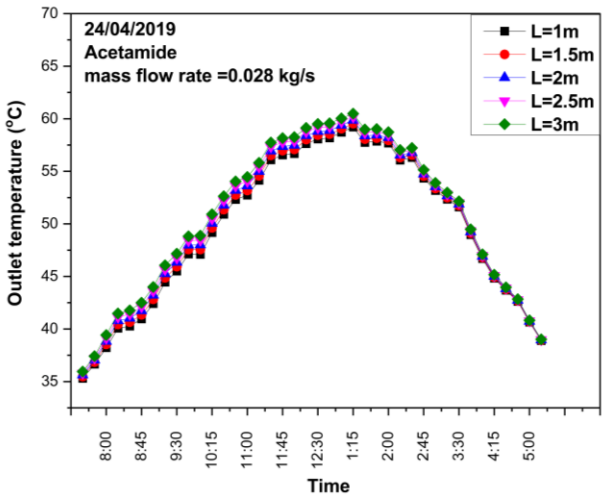

(b)

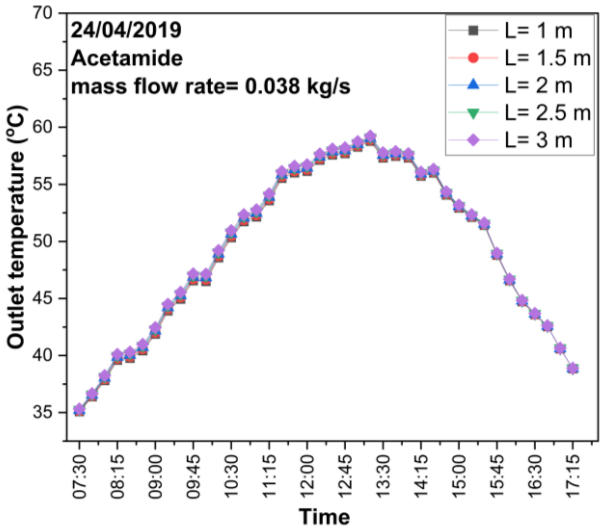

(c)

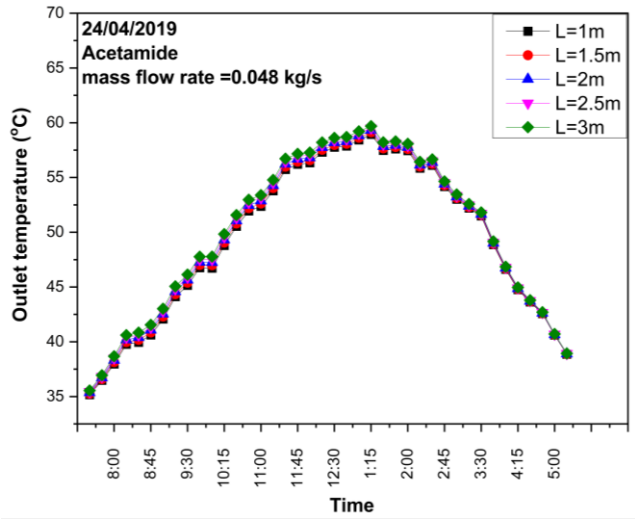

(d)

Fig. 4.6: Theoretical outlet temperature with varying length of absorber and mass flow rates (a) 0.018 kg/s (b) 0.028 kg/s (c) 0.038 kg/s and (d) 0.048 kg/s with acetamide as PCM

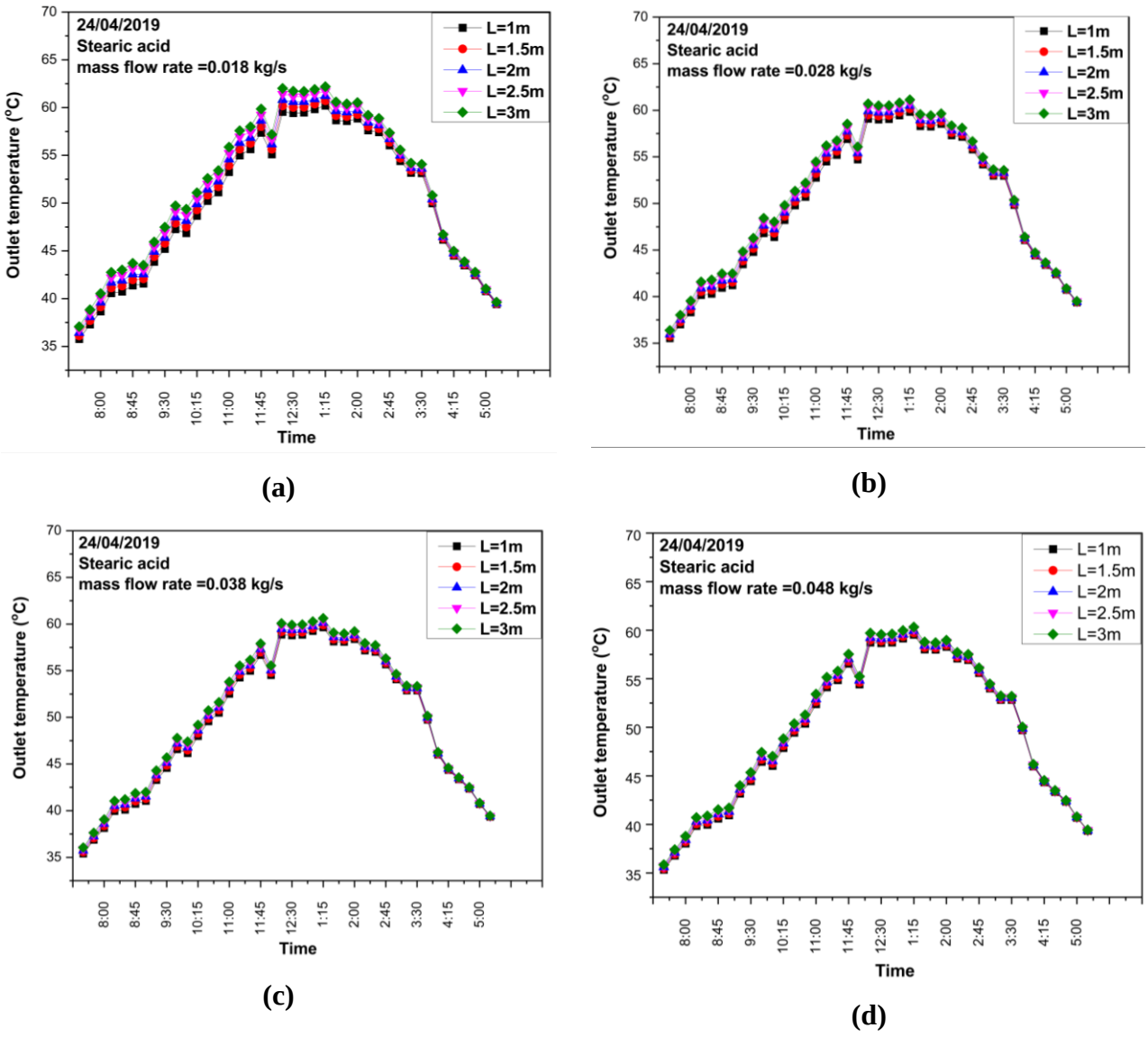

Fig. 4.7: Theoretical outlet temperature with varying length of absorber and mass flow rates (a) 0.018 kg/s (b) 0.028 kg/s (c) 0.038 kg/s and (d) 0.048 kg/s with stearic acid as PCM

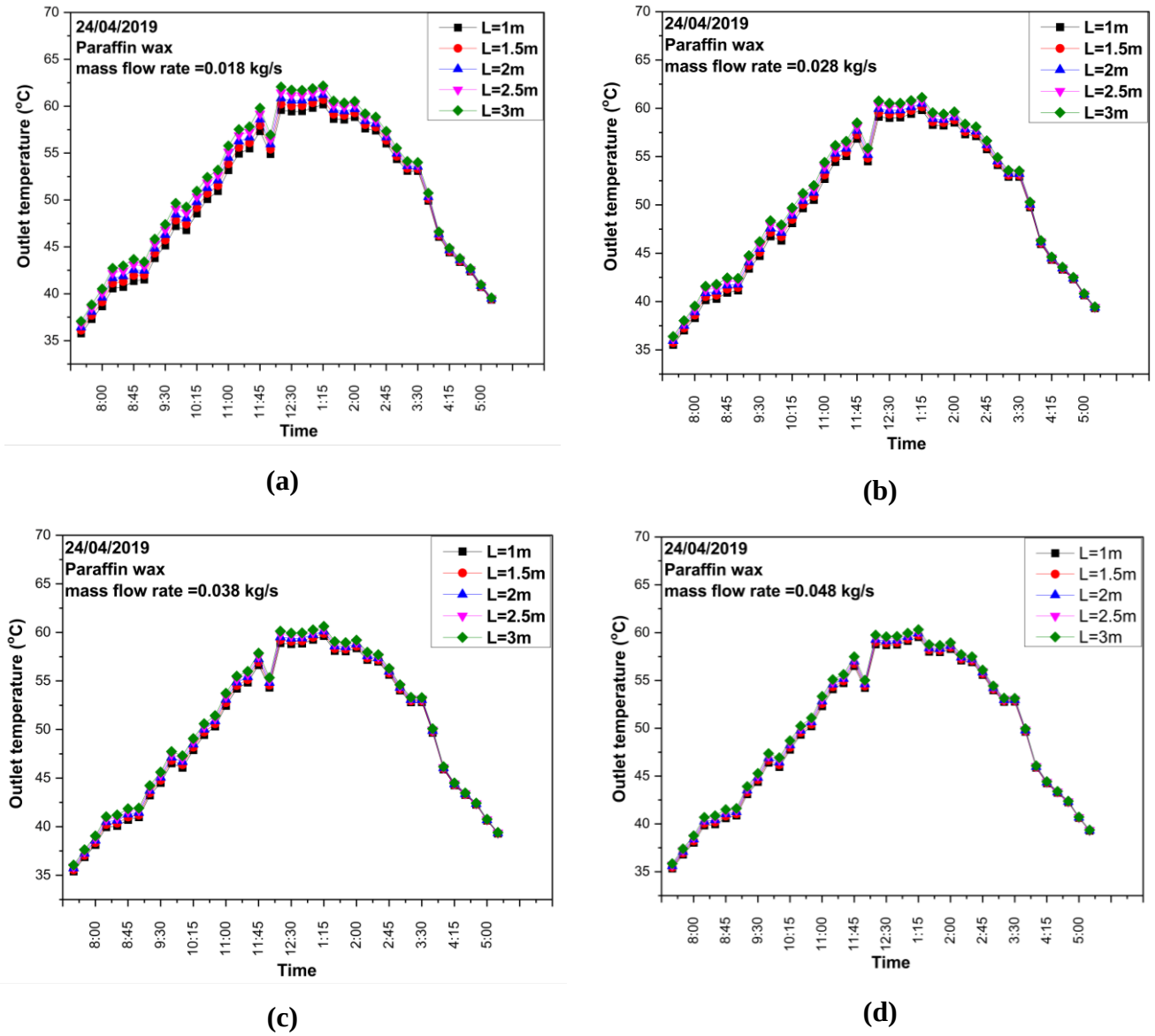

Fig. 4.8: Theoretical outlet temperature with varying length of absorber and mass flow rates (a) 0.018 kg/s (b) 0.028 kg/s (c) 0.038 kg/s and (d) 0.048 kg/s with paraffin wax as PCM

Fig. 4.9 represents the theoretical useful energy with varying air mass flow rate and length of the absorber plate. Highest theoretical useful energy is produced at lowest air mass flow rate (0.018 kg/s) and lowest theoretical useful energy produced at highest air mass flow rate (0.048 kg/s) in case of all the PCMs. However, there is a marginal increase in useful energy with increase in length of the absorber plate.

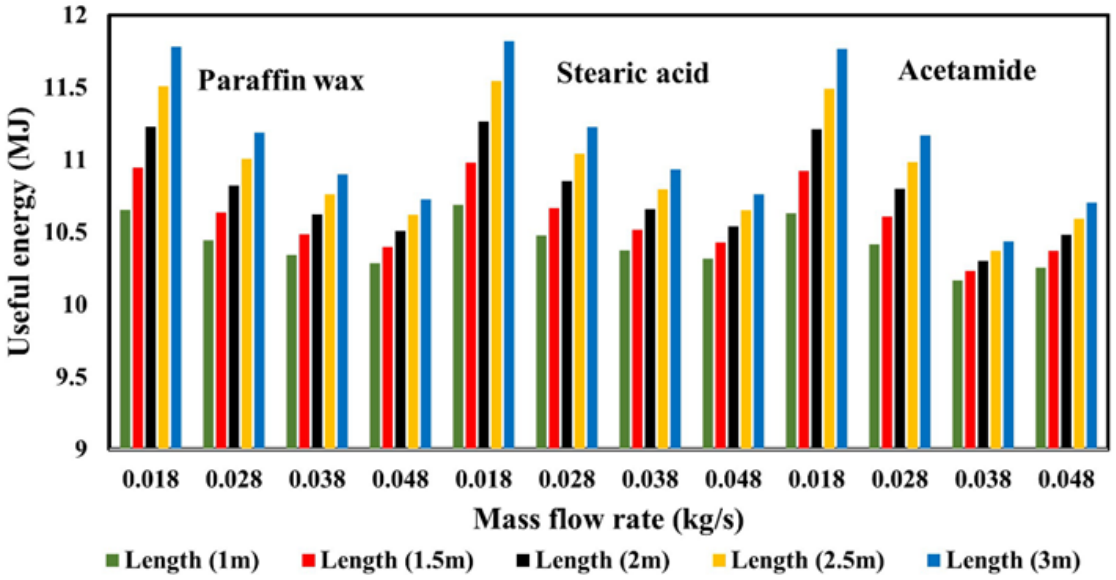

Fig. 4.9: Theoretical useful energy with varying air mass flow rate and length of the absorber plate

From the observation of the (T_{fos}) plot and theoretical useful energy plot it can be decided that the lowest air mass flow rate 0.018 kg/s produced highest theoretical outlet temperature and useful energy also since there is negligible change in theoretical outlet temperature difference and theoretical useful energy with the increase in length from 1 to 3 m for all the PCMs. Finally, 1.57 m and 0.018 kg/s as absorber plate length and air mass flow rate are considered for the present study.

4.3.2 PCM quantity sizing

For PCM cavity sizing, the time constant (τ_c) for various PCM-based SAH is estimated to be 3 h to reach 63.2% of the peak theoretical outlet temperature (T_{fos}) from the beginning of T_{fos}, which may be utilised to quantify the depth of the melted PCM. The values of the parameters used in sizing of PCM cavity for three different PCMs are tabulated in Table 4.4. Now these parameters are considered for solving Eq. (4.47) in determining the PCM melting depth as shown in Fig. 4.10.

Table 4.4: Parameters considered for PCM melting depth estimation with different operation conditions for three different PCMs

PCM	ρ_{PCM} *(kg/ m^3)*	L_{st} *(kJ/ kg)*	I *(kW/ m^2)*	C_p *(kJ/k gK)*	T_o *(K)*	T_{in} *(K)*	U_t *(kW/ m^2K)*	U_b *(kW/ m^2K)*	T_p *(K)*	T_a *(K)*	A_p *(m^2)*	$\dot{m}$ *(kg/s)*	τ_c *(s)*
Acetamide	1159	210	0.938	1.007	343	311	5.607 E-05	0.000 22	373	309	(1 – 3) m^2 with 0.5 increment	(0.018-0.048) kg/s with 0.01 increment	108 00
Stearic acid	1080	200. 7	0.938	1.007	343	311	5.607 E-05	0.000 22	373	309	(1 – 3) m^2 with 0.5 increment	(0.018 - 0.048) kg/s with 0.01 increment	108 00
Paraffin wax	818	198. 7	0.938	1.007	343	311	5.607 E-05	0.000 22	373	309	(1 – 3) m^2 with 0.5 increment	(0.018 - 0.048) kg/s with 0.01 increment	108 00

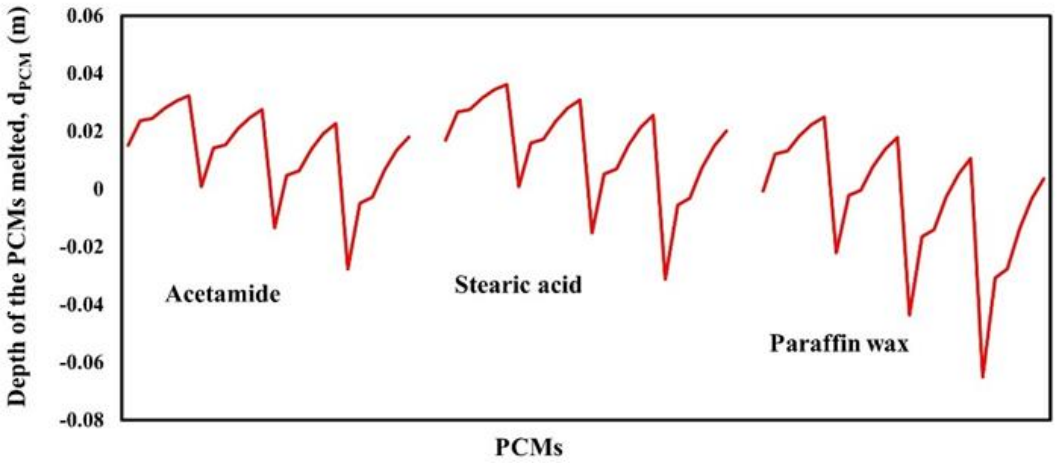

Fig. 4.10: Depth of the PCM melt for varying air mass flow rate and absorber plate area

The depth of the PCM melting ranges from (-2.77 cm to 3.22 cm) for acetamide, (-3.12 cm to 3.62 cm) for stearic acid and (-6.50 cm to 2.49 cm) for paraffin wax matrix an average of 1.30 cm for acetamide, 1.46 cm for stearic acid and -0.38 cm for paraffin wax. Finally, 1 cm is considered for height of the PCM cavity with 1 m breadth and 1.57 m length matrix a total volume of PCM cavity (absorber plate chamber) as 0.0157 m^3. The total mass of PCM required for PCM cavity is presented in Table 4.5 where it is found that

14.56 kg of acetamide, 12.12 kg of stearic acid and 11.30 kg of paraffin wax respectively are required as a LHS unit. Studies carried out by Verma et al. [28] and Summers et al. [21] found optimum PCM thickness as 2 cm and 8 cm that can produce maximum outlet temperature of 60 ºC and 58 ºC.

Table 4.5: Amount of PCM required for PCM cavity

PCM	Density (kg/m^3)	Mass of PCM (kg)	80% of Mass of PCM to be kept inside PCM cavity (kg)
Acetamide	1159	18.212	14.569
Stearic acid	1080	15.150	12.120
Paraffin wax	818	14.130	11.304

4.3.3 Development of PCMSAH based on simulation outcome

Based on the parametric study to optimise the length, mass flow rate, and mass of the PCMs from the preceding sections, two identical solar hot air generators (SAH) are developed locally in the Department of Energy, Tezpur University. The detailed specifications of the SAH are described in Table 4.6.

Table 4.6: Specifications of PCMSAH

S.No.	Specifications	Values
1.	Structure and base material	Wooden frame
2.	Area of absorber plate	1.57 m^2
3.	Material of the PCM cavity	Aluminium
4.	Material of the glass	Float glass type
5.	Glass thickness	0.005 m
6.	Glass area	2 m^2
7.	Glass to absorber plate gap	10mm
8.	Insulation material	Foam and ply board support
9.	Material of SAH outer cover	Aluminium sheet
10.	Air vent area	1 m × 0.1 m
11.	Hot air channel material	PVC suction hose
12.	Mode of air flow	Single pass and overflow
13.	Air blower	Centrifugal blower

The front view, side view and schematic of SAH are shown in Fig. 4.5 (a), (b) and (c). The absorber plates are maintained at a gap of 10cm lengthwise and 6cm breadthwise insulated from for receiving maximum amount of solar radiation through the exposed glass area which can be seen in Fig. 4.11 (a) and (b).

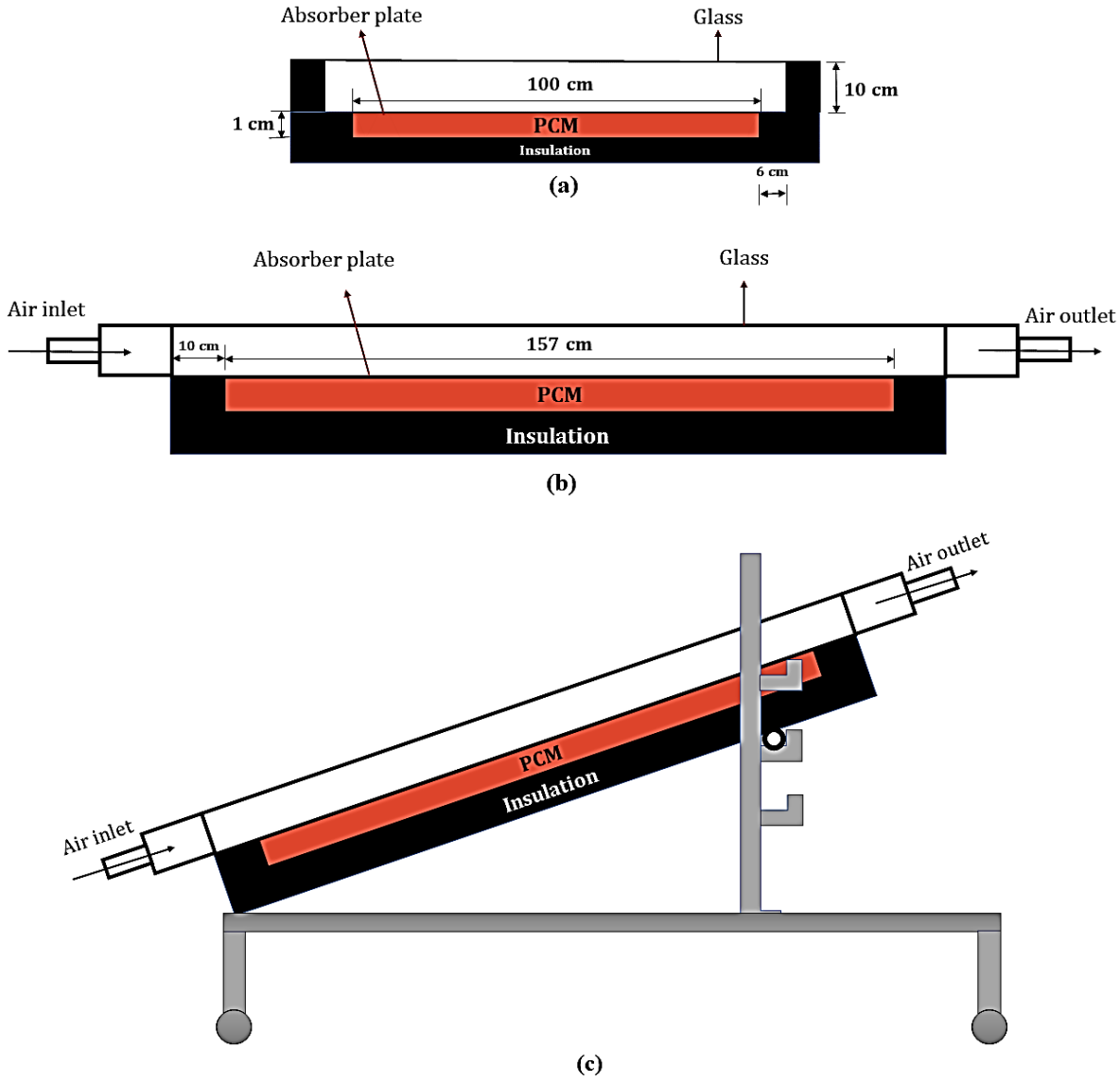

Fig. 4.11: (a) Front view of SAH breadth wise. (b) side view of SAH length wise. (c) schematic of SAH with support and stand

4.3.4 Comparison of performance of SAH (with and without PCM)

The experiments are conducted on clear sunny days during the period of April to July 2021(07:30 AM – 05:15 PM) for three different PCMs respectively. The outlet temperature of two identical SAH one with PCM and other without PCM along with

ambient temperature are shown in Fig. 4.12. The solar radiation and the PCM plate temperature for different PCM is presented in Fig. 4.12. The maximum drop in outlet temperature during charging operation is resulted by paraffin wax (6.09 ºC) followed by stearic acid (5.44 ºC) and acetamide (3.33 ºC) in comparison with the SAH without PCM. However, trend is different during discharge mode of operation as evidenced by the maximum gain in outlet air temperature with stearic acid (9.57 ºC) followed by paraffin wax (6.48 ºC) and acetamide (1.73 ºC) in comparison to the SAH without PCM. The outlet temperature of PCMSAH can be noticed to be lower than SAH during the charging period but higher during the discharging period and low radiation period. The plate temperature of the stearic acid reached highest during the experiment followed by paraffin wax and acetamide corresponding to the respective solar radiations as shown in Fig. 4.13.

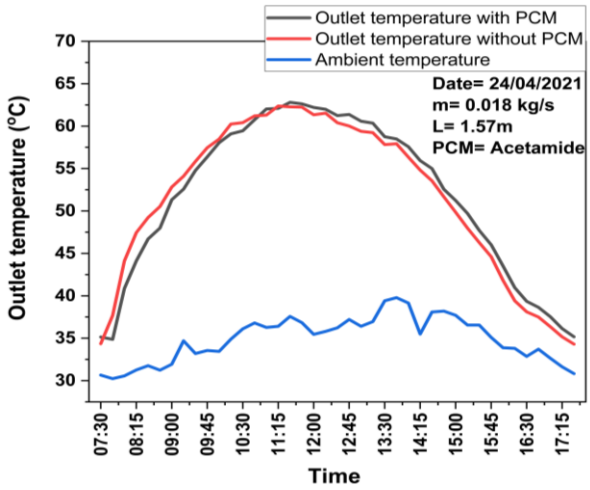

(a)

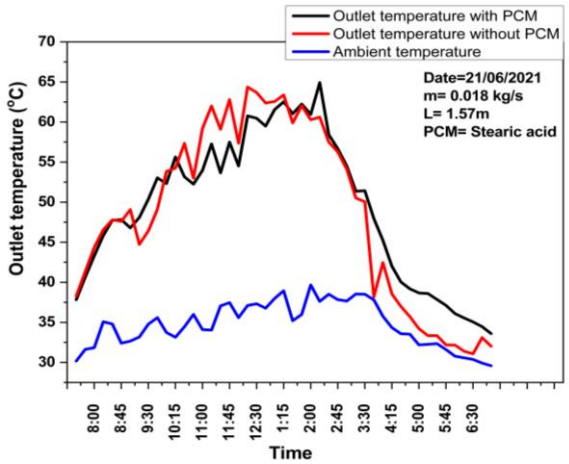

(b)

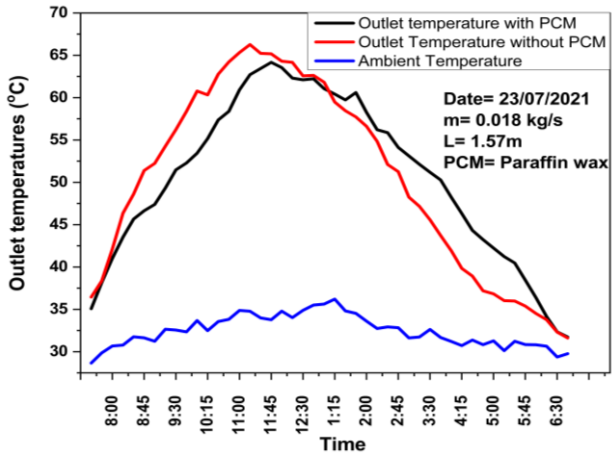

(c)

Fig. 4.12: Experimental outlet temperature of SAH with (a) acetamide (b) stearic acid (c) paraffin wax PCMs and without PCM

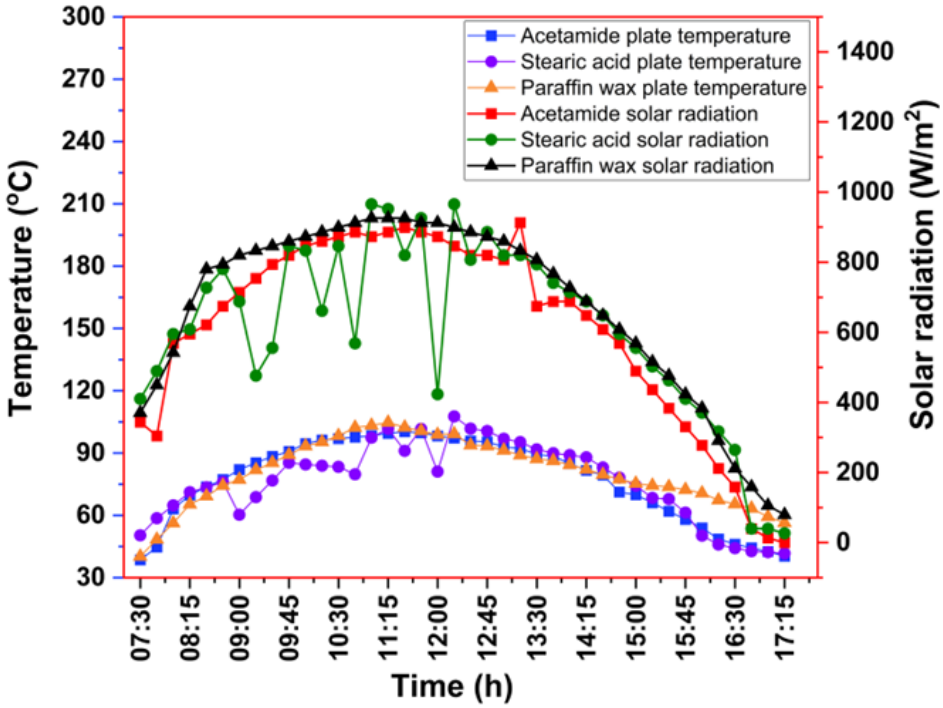

Fig. 4.13: Solar Radiation and Plate temperature for SAH with three different PCMs

Fig. 4.14 (a), (b) and (c) represents the validation of parametric study for theoretical outlet temperature *(T_{fos})* with experimental outlet temperature of PCMSAH using three different PCMs: acetamide, stearic acid, and paraffin wax. The theoretical and experimental outlet temperatures are validated using 15 % deviation and found in close agreement with each other. Moreover, the mean relative error between experimental and theoretical outlet

temperature for three different PCMs are found to be within acceptable limit such as 4.50 % (paraffin wax), 2.32 % (stearic acid) and 2.63 % (acetamide) respectively.

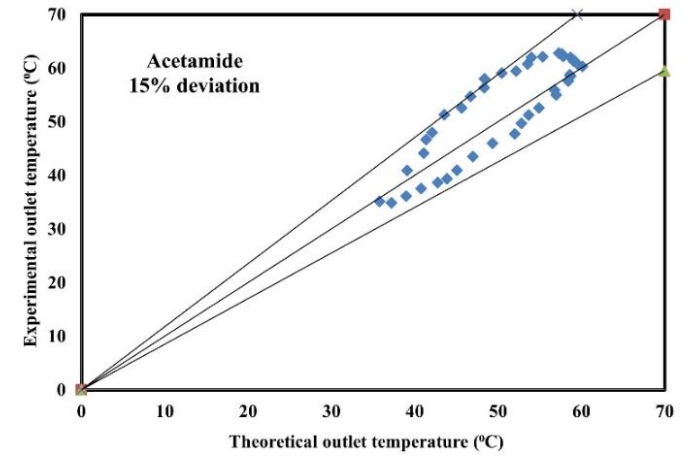

(a)

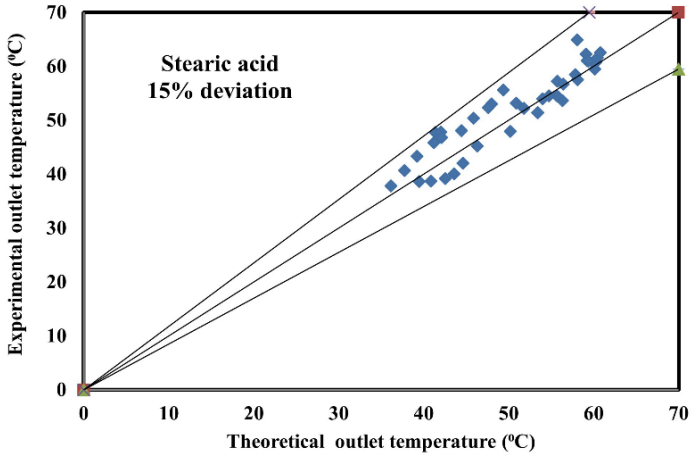

(b)

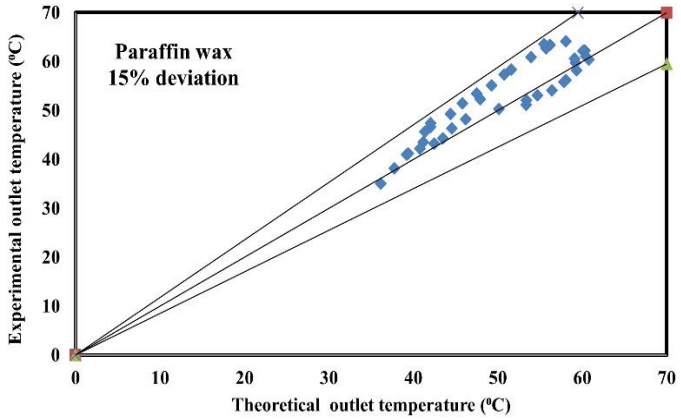

(c)

Fig. 4.14: Theoretical and experimental outlet temperatures of PCMSAH with (a) acetamide, (b) stearic acid and (c) paraffin wax

4.3.5 Energy analysis of SAH (with and without PCM)

The trend of the absorbed, useful, lost, and stored energy is presented in Fig. 4.15 (a), (b) and (c) for three days April 24th, June 21st, and July 23rd, 2021. The energy balance equation, Eqs. (4.1), (4.2), (4.3) and (4.4) are used to evaluate the absorbed, useful, lost, and stored heat. The absorbed, useful, lost, and stored heat of acetamide attained during the experiment are calculated as 33230.2 W, 11576.9 W, 752.49 W and 20900.8 W respectively. Similarly for stearic acid the absorbed, useful, lost, and stored heat are respectively 33427.54 W, 10655.09 W, 724.46 W and 22047.98 W respectively. Subsequently for paraffin wax the absorbed, useful, lost, and stored heat are estimated as 36567.54 W, 14135.18 W, 838.24 W and 21594.12 W respectively. During the experiment, PCMSAH with paraffin wax produced the most useable heat of around 14kW. The absorbed, useful, and stored heat is higher in case of all the PCMs as compared to study carried out by Khadraoui et al. [29] despite having a larger collector area of 2.12 m^2. The stored heat in the PCM cavity of the current study is around (59 % to 66 %) and 70 % in the study carried out by Khadraoui et al. [29].

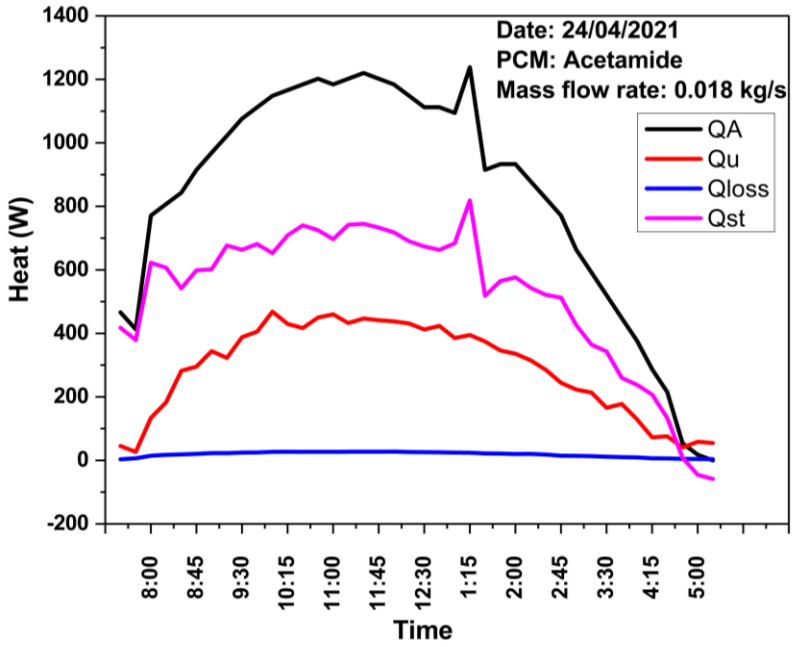

(a)

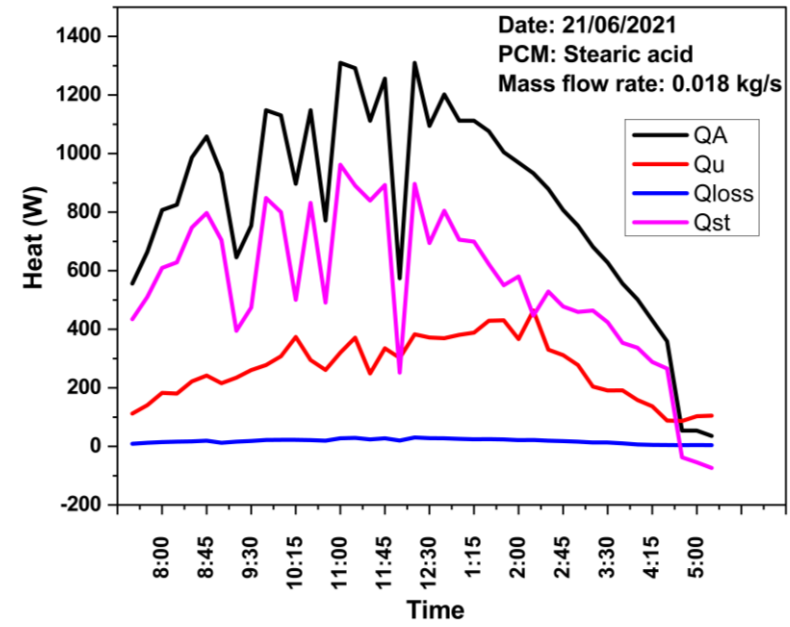

(b)

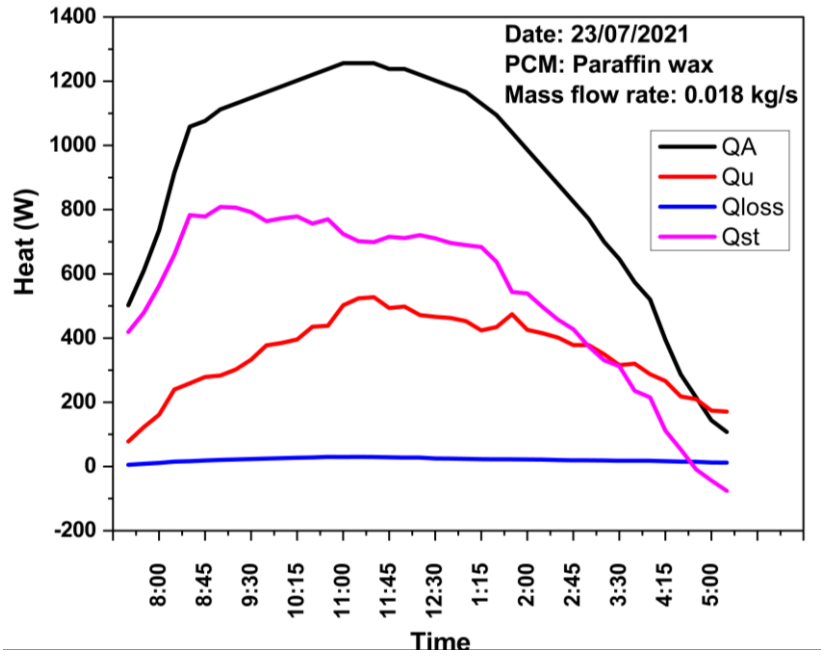

(c)

Fig. 4.15: Absorbed, useful, lost and stored heat of the SAH with (a) acetamide (b) stearic acid and (c) paraffin wax as PCM

Fig. 4.16 represents the performance comparison of the SAH (with and without PCM) in terms of different types of energy involve during the experiments. Marginal rise in useful heat produced by PCMSAH is attained with acetamide (1.7 %) followed by paraffin wax (0.79 %) and stearic acid (0.34 %) in comparison of the SAH without PCM. The highest

amount of heat is stored with stearic acid (65.95 %) followed by acetamide (62.889 %) and paraffin wax (59.05 %).

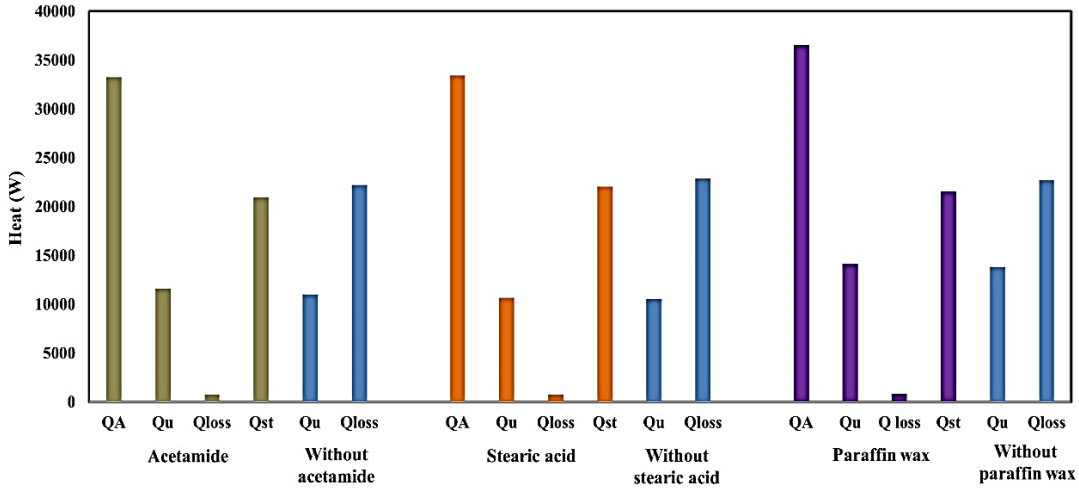

Fig. 4.16: Absorbed, useful, lost, and stored heat of the SAH with (a) acetamide (b) stearic acid and (c) paraffin wax

In terms of daily average thermal efficiency, paraffin wax (45.64 %) based SAH ranks first followed by stearic acid (45.20 %) and acetamide (40.83 %). PCMSAH with stearic acid stands 13.04 % higher to the SAH without PCM, similarly PCMSAH with paraffin wax remained 7.07% and acetamide 5.77 % higher to the SAH without PCM respectively. Khadraoui et al. [29] carried out an experimental investigation on SAH integrated with rectangular cavity filled with Paraffin wax in Tunisia (Longitude 10.42 ºE, Latitude 36.72 ºN). The energy efficiency from the experiment on different days are found to be 32.85 % (27/08/2015) and 34.19 % (28/08/2015).

4.3.6 Uncertainty analysis for thermal efficiency of PCMSAH

The uncertainty analysis is carried out to determine the accuracy of the experiments performed on the PCMSAH. In this study, the errors came from the sensitiveness of equipment and the measurements uncertainties. The independent parameters measured in the experiments reported here are (i) collector inlet and outlet temperature, (ii) ambient temperature, (iii) PCM temperature, (iv) air velocity, and (v) solar radiation.

$$\Delta y = \pm\sqrt{(\frac{\partial y}{\partial x_1}\Delta x_1)^2 + (\frac{\partial y}{\partial x_2}\Delta x_2)^2 + \cdots \ldots \ldots \ldots \ldots (\frac{\partial y}{\partial x_n}\Delta x_n)^2} \quad (4.48)$$

where, Δy is the uncertainty in the evaluated dependent variable and $\Delta x_1, \Delta x_2, \ldots \ldots, \Delta x_n$ are the independent variable errors [30, 31].

Finally, the uncertainty of the thermal efficiency of PCMSAH for the present study is given by.

$$\Delta\eta_T = \pm\sqrt{(\frac{\partial\eta_T}{\partial\dot{m}}\Delta\dot{m})^2 + (\frac{\partial\eta_T}{\partial T_o}\Delta T_o)^2 + (\frac{\partial\eta_T}{\partial T_i}\Delta T_i)^2 + (\frac{\partial\eta_T}{\partial I}\Delta I)^2 + (\frac{\partial\eta_T}{\partial A_p}\Delta A_p)^2} \quad (4.49)$$

Where, $\Delta\eta_T$ is the uncertainty associated with the thermal efficiency of the SAH, and $\Delta\dot{m}$, ΔT_o, ΔT_i, ΔI,ΔA_P are the uncertainties associated with the mass flow rate, outlet temperature, inlet temperature, radiation intensity and area of SAH respectively. The relative errors in measurements of solar radiation, air temperature across the PCMSAH, mass flow rate, absorber plate area, and the uncertainties are shown in Table 4.7. The uncertainty in the thermal efficiency is computed as ±2.02 %.

Table 4.7: Uncertainty of parameters in the measurement

S.No.	Parameter	Value of parameter	Relative error of the instruments	Uncertainty	Remarks
1	Solar radiation	590 W/m^2	±5 W/m^2	±0.03 %	The value of the parameters like solar radiation, and inlet and outlet temperatures are the average value obtained during the experiments.
2	Inlet temperature	36 ºC	±2 ºC	±2.36 %	
3	Outlet temperature	52 ºC	±2 ºC	±1.638 %	
4	Mass flow rate	0.018 kg/s	±1.5%	±0.0546 %	
5	Area of the absorber plate	1.57 m^2	±1%	±0.0036 %	

4.4 Summary

In the present Chapter, we have studied the feasibility of integration of the selected PCMs in the SAH. The effect of mass flow rate of air on the outlet air temperature of SAH was examined by simulations and found that the lowest air mass flow rate (0.018 kg/s) produces highest theoretical outlet temperature 63.27 ºC (acetamide), 60.31 ºC (stearic acid) and 60.40 ºC (paraffin wax) as compared to highest air mass flow rate (0.048 kg/s) that produce 61.51 ºC (acetamide), 58.48 ºC (stearic acid) and 59.35 ºC (paraffin wax) theoretical outlet temperature respectively. With increase in the length of the absorber plate (1 m to 3 m), the highest outlet temperature difference obtained is 2.16 ºC with 0.018 kg/s of air mass flow rate for stearic acid and 0.82 ºC with 0.048 kg/s of air mass flow rate in case of stearic acid and paraffin wax. Therefore, the air mass flow rate of 0.018 kg/s

and length of the absorber plate as 1.57 m are considered from the theoretical studies to develop the two identical SAH (with and without PCM).

The PCM melting depth is estimated with an average melting depth of 1.30 cm for acetamide, 1.46 cm for stearic acid and -0.38 cm for paraffin wax. Therefore, 1 cm of PCM cavity height is considered to find the total mass of PCM required for LHS inside the PCM cavity as 14.56 kg of acetamide, 12.12 kg of stearic acid and 11.30 kg of paraffin wax respectively.

During the investigation of performance comparison of SAH with and without PCM it is found that the maximum outlet temperature difference obtained during charging period is 3.33 °C for acetamide, 5.44 °C for stearic acid and 2.89 °C for paraffin wax and subsequently the maximum outlet temperature difference acquired during discharging period is found to be 1.73 °C for acetamide, 9.75 °C for stearic acid and 6.56 °C for paraffin wax. The major advantage of the PCMSAH is the uniform outlet temperature during discharging process and higher outlet temperatures with comparison to SAH without PCM for a longer period.

The validation between the theoretical and experimental outlet temperature showed close agreement for all the PCMs and the mean relative error are within acceptable limit such as 4.50 % (paraffin wax), 2.32 % (stearic acid) and 2.63 % (acetamide) respectively.

The absorbed, usable, lost, and stored heat of acetamide (33230.2 W, 11576.9 W, 752.49 W, and 20900.8 W), stearic acid (33427.54 W, 10655.09 W, 724.46 W, and 22047.98 W) and for paraffin wax (36567.54 W, 14135.18 W, 838.24 W, and 21594.12 W) are obtained during the experiment.

During comparison to SAH without PCM, there is a marginal increase in usable heat produced by PCMSAH with acetamide (1.7 %), paraffin wax (0.79 %), and stearic acid (0.34 %). Stearic acid stored the most heat (65.95 %), followed by followed by acetamide (62.889 %) and paraffin wax (59.05 %).

Paraffin wax based PCMSAH (45.64 %) had the highest thermal efficiency, followed by stearic acid (45.20 %) and acetamide (40.83 %). Stearic acid based PCMSAH thermal efficiency is 13.04 % higher to that of SAH without PCM, followed by paraffin wax is 7.07%, and acetamide is 5.77 % respectively.

The uncertainty in the thermal efficiency of the PCMSAH is computed as ± 2.02%. The novel PCM integrated SAH design will be effective for space heating or solar drying of the local perishable agricultural items which will be discussed in the following Chapter.

References

[1] Duffie, J. A., & Beckman, W. A. Solar Engineering of Thermal Processes. *John Wiley & Sons*, New York, 1991.

[2] Kalogirou, S. A. Solar thermal collectors and applications. *Progress in energy and combustion science*, 30(3): 231-295, 2004.

[3] Tiwari, G.N. Solar Energy, *Narosa Publishing house*, New Delhi, 2002.

[4] Saini, R. P., & Singal, S. K. A review on roughness geometry used in solar air heaters. *Solar energy*, 81(11): 1340-1350, 2007.

[5] Arunkumar, H. S., Karanth, K. V., & Kumar, S. Review on the design modifications of a solar air heater for improvement in the thermal performance. *Sustainable Energy Technologies and Assessments*, 39: 100685, 2020.

[6] Alkilani, M. M., Sopian, K., Alghoul, M. A., Sohif, M., & Ruslan, M. H. Review of solar air collectors with thermal storage units. *Renewable and Sustainable Energy Reviews*, *15*(3): 1476-1490, 2011.

[7] Kabeel, A. E., Khalil, A., Shalaby, S. M., & Zayed, M. E. Improvement of thermal performance of the finned plate solar air heater by using latent heat thermal storage. *Applied Thermal Engineering*, 123: 546-553, 2017.

[8] Madhulatha, G., Kumar, M. M. J., & Sateesh, P. Optimization of tube arrangement and phase change material for enhanced performance of solar air heater-A numerical analysis. *Journal of Energy Storage*, 41: 102876, 2021.

[9] Omojaro, A. P., & Aldabbagh, L. B. Y. Experimental performance of single and double pass solar air heater with fins and steel wire mesh as absorber. *Applied energy*, 87(12): 3759-3765, 2010.

[10] Liu, C., Wu, Y., Li, D., Zhou, Y., Wang, Z., & Liu, X. Effect of PCM thickness and melting temperature on thermal performance of double glazing units. *Journal of Building Engineering*, 11: 87-95, 2017.

[11] Sengupta, M., Perez, R., Gueymard, C., Anderberg, M., & Gotseff, P. Satellite-Based Solar Resource Data Sets for India 2002-2012. Technical Report no. NREL/TP-5D00-61121, National Renewable Energy Lab. (NREL), Golden, CO (United States), 2014.

[12] El Khadraoui, A., Bouadila, S., Kooli, S., Guizani, A., & Farhat, A. Solar air heater with phase change material: An energy analysis and a comparative study. *Applied Thermal Engineering*, 107:1057-1064, 2016.

[13] Buchberg, H., Ivan Catton, and D. K. Edwards. Natural convection in enclosed spaces—a review of application to solar energy collection. *ASME Journal of Heat and Mass Transfer*, 182-188. 1976.

[14] Karwa, R., & Srivastava, V. Thermal performance of solar air heater having absorber plate with v-down discrete rib roughness for space-heating applications. *Journal of Renewable Energy*, 2013.

[15] Aboul-Enein, S., El-Sebaii, A. A., Ramadan, M. R. I., & El-Gohary, H. G. Parametric study of a solar air heater with and without thermal storage for solar drying applications. *Renewable energy*, 21(3-4):505-522, 2000.

[16] Jelle, B. P., & Gustavsen, A. Solar radiation glazing factors for electrochromic windows for building applications. Proceedings of Building Enclosure Science & Technology BEST 2, 2010.

[17] Muthu, G., Shanmugam, S., & Veerappan, A. R. Solar parabolic dish thermoelectric generator with acrylic cover. Energy Procedia, 54, 2-10, 2014.

[18] https://www.engineeringtoolbox.com/thermal-conductivity-d_429.html (Accessed on 24/03/2021).

[19] Raghu, O., & Philip, J. Thermal properties of paint coatings on different backings using a scanning photo acoustic technique. Measurement science and technology, 17, 11, 2945, 2006.

[20] https://www.thermoworks.com/emissivity-table/ (Accessed on 24/03/2021).

[21] Summers, E. K., & Antar, M. A. Design and optimization of an air heating solar collector with integrated phase change material energy storage for use in humidification–dehumidification desalination. *Solar Energy*, 86(11): 3417-3429, 2012.

[22] Zhu, T. T., Zhao, Y. H., Diao, Y. H., Li, F. F., & Deng, Y. C. Experimental investigation on the performance of a novel solar air heater based on flat micro-heat pipe arrays (FMHPA). *Energy procedia*, 70:146-154, 2015.

[23] Haji-Sheikh, A., Eftekhar, J., & Lou, D. Some thermophysical properties of paraffin wax as a thermal storage medium. In *3rd Joint Thermophysics, Fluids,*

Plasma and Heat Transfer Conference, page 846, St. Louis, United States of America, 1982.

[24] Brahma, B., Narzary, R., & Baruah, D. C. Acetamide for latent heat storage: Thermal stability and metal corrosivity with varying thermal cycles. *Renewable Energy*, 145: 1932-1940, 2020.

[25] Sharma, A., Tyagi, V. V., Chen, C. R., & Buddhi, D. Review on thermal energy storage with phase change materials and applications. *Renewable and Sustainable energy reviews*, 13(2):318-345, 2009.

[26] Sari, A., & Kaygusuz, K. Thermal energy storage system using stearic acid as a phase change material. *Solar energy*, 71(6):365-376, 2001.

[27] Chandra, R., & Sodha, M. S. Testing procedures for solar air heaters: a review. *Energy Conversion and Management*, 32(1):11-33, 1991

[28] Verma, G., Singh, S., Chander, S., & Dhiman, P. Numerical investigation on transient thermal performance predictions of phase change material embedded solar air heater. *Journal of Energy Storage*, 47:103619, 2022.

[29] El Khadraoui A, Bouadila S, Kooli S, Guizani A, Farhat A. Solar air heater with phase change material: An energy analysis and a comparative study. *Applied Thermal Engineering*. 107: 1057-1064, 2016.

[30] J.P. Holman, Experimental methods for engineers. <https://mech.at.ua/HolmanICS.pdf>, 2021. Accessed on 03.08.2021.

[31] Heydari, A., & Mesgarpour, M. Experimental analysis and numerical modeling of solar air heater with helical flow path. *Solar Energy*, 162: 278-288, 2018.